CONTRAST MEDIA & MOLECULAR IMAGING

Received: 15 July 2011, Revised: 15 January 2012, Accepted: 28 January 2012, Published online in Wiley Online Library: 2012

(wileyonlinelibrary.com) DOI: 10.1002/cmmi.1465

Labelling of olfactory ensheathing cells with micron-sized particles of iron oxide and detection by MRI

Ioanna Sandvig[a]*, Linh Hoang[b], Thomas C. P. Sardella[c], Susan C. Barnett[c], Christian Brekken[a], Kåre Tvedt[b], Martin Berry[d], Olav Haraldseth[a], Axel Sandvig[a,e,f] and Marte Thuen[a]

A crucial issue in transplant-mediated repair of the damaged central nervous system (CNS) is serial non-invasive imaging of the transplanted cells, which has led to interest in the application of magnetic resonance imaging (MRI) combined with designated intracellular magnetic labels for cell tracking. Micron-sized particles of iron oxide (MPIO) have been successfully used to track cells by MRI, yet there is relatively little known about either their suitability for efficient labelling of specific cell types, or their effects on cell viability. The purpose of this study was to develop a suitable MPIO labelling protocol for olfactory ensheathing cells (OECs), a type of glia used to promote the regeneration of CNS axons after transplantation into the injured CNS. Here, we demonstrate an OEC labelling efficiency of >90% with an MPIO incubation time as short as 6 h, enabling intracellular particle uptake for single-cell detection by MRI without affecting cell proliferation, migration and viability. Moreover, MPIO are resolvable in OECs transplanted into the vitreous body of adult rat eyes, providing the first detailed protocol for efficient and safe MPIO labelling of OECs for non-invasive MRI tracking of transplanted OECs in real time for use in studies of CNS repair and axon regeneration. Copyright © 2012 John Wiley & Sons, Ltd.

Keywords: contrast agents; magnetic particles; intracellular labels

1. INTRODUCTION

MRI is widely used to study central nervous system (CNS) damage and repair both in basic research and in the clinic. Traditionally, MRI has described post-injury physioanatomical changes, but in the last few years its use has been extended to serial and non-invasive imaging of the behaviour of cells implanted into the CNS to control scarring and promote axon regeneration (1). Different magnetic particles are available for intracellular labelling and visualization of cell grafts, including superparamagnetic iron oxides (SPIO) and ultra-small superparamagnetic iron oxides (USPIO), both of which have been used in a number of MRI studies (1–6). However, very large numbers of SPIO/USPIO are required for efficient cell detection by MRI, a shortcoming that is resolved by using micron-sized particles of iron oxide (MPIO), which have a higher magnetite content than SPIO/USPIO, so that attenuation of the MR R_2* relaxivity contrast is significantly increased after endocytosis of only a few particles (7–11).

Olfactory ensheathing cells (OECs) are glia that enwrap bundles of the unmyelinated axons of olfactory receptor neurons from the olfactory mucosa, through the cribriform plate and into the olfactory bulb glomeruli (12). In the last decade, OECs have been transplanted into the injured CNS to promote repair, resulting in the emergence of OECs as glia with reparative properties, including the secretion of neurotrophins, the promotion of both regeneration and remyelination of damaged axons (13–15), and the improvement of functional recovery after spinal cord injury (16,17). Furthermore, the findings of these studies indicate that OECs may also be utilized as intravitreal transplants for neuroprotection and/or regeneration of retinal ganglion cell axons, as an alternative to peripheral nerve grafts after optic nerve injury (18–20). Clearly, the study of the behaviour of implanted OECs in experimental CNS injury models will benefit from non-invasive imaging documenting graft/host temporospatial integration. Although investigators have already used this

* *Correspondence to: Ioanna Sandvig, Department of Circulation and Medical Imaging, Medical Technical Research Centre, NTNU, 7489 Trondheim, Norway. Email: ioanna.sandvig@ntnu.no*

a *I. Sandvig, C. Brekken, O. Haraldseth, A. Sandvig, M. Thuen*
MI Lab and Department of Circulation and Medical Imaging, Norwegian University of Science and Technology, Trondheim, Norway

b *L. Hoang, K. Tvedt*
Department of Laboratory Medicine and Children's and Women's Health, Norwegian University of Science and Technology, Trondheim, Norway

c *T.C.P. Sardella, S.C. Barnett*
College of Medical, Veterinary and Life Sciences, University of Glasgow, Scotland, UK

d *M. Berry*
Molecular Neuroscience, Division of Medical Sciences, Institute of Biomedical Research, University of Birmingham, Birmingham, UK

e *A. Sandvig*
Department of Neurosurgery, Umeå University Hospital, Umeå, Sweden

f *A. Sandvig*
Laboratory of Regenerative Neurobiology, Department of Laboratory Medicine, Children's and Women's Health, Norwegian University of Science and Technology, Trondheim, Norway

approach (21,22), *in vivo* MRI of transplanted OECs is still in its infancy and little is known about potential MPIO cytotoxicity.

In this study, we labelled OECs intracellularly with 0.96 μm diameter MPIO and used *in vitro* assays to assess the viability, proliferation and migration of MPIO-labelled OECs. We demonstrate that MPIO are avidly endocytosed by OECs in culture, without compromising cell viability, and have detected MPIO-labelled OECs by MRI at 7 T *in vitro*. Furthermore, we have detected MPIO-labelled OEC transplanted into the vitreous body of adult rats by MRI *in vivo*. We thus provide proof-of-principle for the suitability of our protocol for labelling OECs with MPIO, thereby justifying the use of MRI for *in vivo* tracking of transplanted MPIO-labelled OECs in the CNS.

2. MATERIALS AND METHODS

2.1. Cell isolation, culture and labelling

2.1.1. OEC purification and culture

Neonatal OECs were purified as described by Barnett and Roskams (23). Briefly, the olfactory bulbs of P7 Fischer rats (typically from four or five animals) were finely chopped with a scalpel, enzymatically digested in L-15 (Leibovitz) medium (Sigma) and triturated through a 26-gauge needle. Dissociated cells were incubated in a cocktail of primary antibodies consisting of the O4 monoclonal (IgM at 1:4) and the monoclonal anti-galactocerebroside (IgG3 at 1:2), followed by their fluorochrome conjugated class-specific secondary antibodies. Following rinses, dissociated cells were incubated in secondary antibodies consisting of goat anti-mouse IgM phycoerythrin and goat anti-mouse IgG3 fluorescein (1:100, Southern Biotech). OECs were purified by fluorescence-activated cell sorting (FACS, Vantage Becton Dickenson) by selecting for galactocerebroside-negative and O4-positive cells. OECs were subsequently cultured in Dulbecco's modified Eagle's medium (DMEM GlutaMAX; Sigma) with 1.25% gentamicin (Sigma) and 5% FBS (Autogen Bioclear) on 13 $\mu g\,ml^{-1}$ poly-L-lysine- (PLL; Sigma) coated 25 cm^2 flasks. The cultures were supplemented with 500 $ng\,ml^{-1}$ fibroblast growth factor 2 (FGF2; Peprotech, London, UK), 50 $ng\,ml^{-1}$ heregulin (hrgβ1; R&D Systems Europe Ltd, Abingdon, UK), and 10^{-6} M forskolin (Sigma). OECs were passaged at confluence and harvested after six passages. Purity of the OEC populations was assessed by p75 neurotrophin receptor specific labelling and was always 98–100%.

2.2. Contrast agent

OECs were labelled intracellularly with MPIO microspheres 0.96 μm in diameter, comprising a COOH-modified styrene–divinyl benzene inert polymer with an Fe_3O_4 magnetic core (27.8% w/w magnetite content) and a fluorescent label (Dragon Green; excitation 480, emission 520; MC05F/8112; density 2.06 g cm^{-3}, 1% solids, 1.278×10^{10} beads ml^{-1}; Bangs Laboratories Inc., Fishers, IN, USA). The MPIO were washed with and resuspended in PBS and subsequently added to OEC cultures and co-incubated at 37 °C for 6–18 h at concentrations of 10:1, 20:1, 50:1, and 100:1, corresponding to approximately 1.2, 2.4, 6 and 12 pg of iron per cell. Unlabelled OEC cultures at the same stage of confluence were used as controls.

2.3. Cell proliferation, viability and migration

After labelling with MPIO, OEC proliferation was measured after the conversion of resazurin to resorufin, using AlamarBlue® reagent (Invitrogen) as 10% of sample volume and reading absorbance (maximum 570 nm) on a Wallac microwell plate reader (Perkin Elmer) after a 4 h incubation. In addition, OEC viability was evaluated by measuring calcein vs ethidium homodimer-1 expression with LIVE/DEAD® assay (Invitrogen). All of the above assays were performed at 24, 48, 72 and 96 h after labelling. Labelled cell cultures were subsequently passaged. Cell migration was assessed by observing the movement of cells across an undisturbed PLL-coated culture surface and, also across a 2 mm-wide cell-free, rough-surfaced gap, created by scratching through the cell monolayer across the diameter of the dish with a sterile glass micropipette. Cells were manually counted on either side of the gap at 24, 48, 72 and 96 h.

3. INTRAVITREAL OEC TRANSPLANTATION

Unilateral injections of a 3 μl suspension of 2.5×10^5 MPIO-labelled OECs were made into the left vitreous body of anaesthetized animals, immediately posterior to the ora serrata, using a pulled-glass capillary micropipette with a tip diameter of ~0.1–0.2 mm (Harvard Apparatus). To minimize reflux, the tip of the micropipette remained inside the vitreous body for a few seconds, before being slowly withdrawn. Unlabelled OECs were injected into the contralateral vitreous in the same manner as for MPIO-labelled OECs.

3.1. *In vitro* and *in vivo* MRI

For *in vitro* MRI, phantoms were made containing (i) MPIO and (ii), magnetically labelled cells, by suspending MPIO and MPIO-labelled OECs, respectively, in 2 ml Eppendorf tubes containing warm 1% agarose gel. Different phantoms were made for suspensions of 1.75×10^5, 1.25×10^5, 7.5×10^4, 2.5×10^4, 1.75×10^5, 5×10^3, 5×10^2, 2.5×10^2 and 5×10 MPIO and MPIO-labelled cells. Care was taken to contain the MPIO and MPIO-labelled cell suspension to be imaged within a designated volume inside each Eppendorf in register with the area of maximum sensitivity of the surface coil. The phantoms were imaged on a 7 T Bruker Biospec Avance 70/20 (Bruker Biospin MRI, Ettlingen, Germany) using a T_2*-weighted multi-gradient echo sequence with $TR = 1000$ ms, $TE = 10$ (10, 16, 22, 28 ms), flip angle = 30°, FOV = 1.46×1.31 cm^2, acquisition matrix = 128×128, resolution = 114×102 μm per pixel, number of slices = 10, and slice thickness = 0.70 mm (i.e. no gap). The acquisition time was 42 min 40 s with 20 averages. A 72 mm volume resonator was used for RF transmission and an actively decoupled mouse head surface coil for RF reception.

For *in vivo* MRI of intravitreal MPIO-labelled OEC transplants, anaesthetized animals lay prone in a dedicated animal bed heated at 37 °C with circulating water. A multi-gradient echo sequence with $TR = 1000$ ms, $TE = 5$ (5, 10, 15, 20 ms), flip angle = 30%, FOV = 2.8×2.5 cm^2, acquisition matrix = 224×200, resolution = 125×125 μm per pixel, number of slices = 10, slice thickness = 0.70 mm (i.e. no gap) was used. Acquisition time was 16 min 40 s with five averages. A 72 mm volume resonator was used for RF transmission and an actively decoupled mouse head surface coil for RF reception. Water-cooled BGA-12 (400 $mT\,m^{-1}$) gradients were used.

3.2. Electron, transmitted light, DIC, fluorescent and confocal microscopy

MPIO-labelled OECs were pelleted and fixed overnight at room temperature in 2% glutaraldehyde in 0.1 M phosphate buffer

(pH 7.2). The cells were then post-fixed for 1 h in 2% OsO_4 in 0.1 M phosphate buffer (pH 7.2), rinsed with 0.1 M phosphate buffer (pH 7.2), dehydrated through graded ethanol and embedded in Epon resin. Thin (70 nm) sections were cut with an ultramicrotome (Leica 06), collected on copper grids and positive-stained with 4% uranyl acetate (in 50% ethanol) and 1% lead citrate (in 0.2 M NaOH). Sections were examined in a Tecnai 12 transmission electron microscope (TEM; Philips) at 80 kV. Images were captured with a Morada digital camera and processed using iTEM software. Fluorescent and transmitted light images were captured in an Axiovert 40 microscope (Zeiss, Germany). An LSM 510 microscope (Zeiss, Germany) was used for differential interference contrast (DIC) and confocal microscopy.

3.3. Animals

All animal procedures were approved by the appropriate ethics committee in accordance with the national, regional and site guidelines that apply.

4. RESULTS

4.1. Short MPIO incubation times achieved efficient OEC labelling

MPIO were readily endocytosed by OECs and efficient labelling occurred after co-incubation for up to a maximum of 18 h and a minimum of 6 h. MPIO uptake into OECs was evaluated by transmitted light, confocal, fluorescence and TEM (Figures 1–3). Although individual labelled OECs had different levels of uptake of magnetic particles, they all reached labelling efficiencies of >90% after 6 and 18 h of incubation (Fig. 1E and F). The average intracellular iron uptake correlated with the concentrations of MPIO used for the different labelling assays and, based on microscopic assessment, it was estimated to be between ~1.90 and ~13.80 pg, corresponding to a mean range of 12–115 endocytosed MPIO. The MPIO label was retained by the OECs throughout the observation period. An optimal labelling efficiency of >90% was obtained when cultured OECs had reached 50% confluence before MPIO exposure, while labelling efficiency using sub-confluent or confluent OEC cultures was significantly compromised, i.e. little or no MPIO uptake was observed, irrespective of incubation time (data not shown).

4.2. OEC viability and migration was not compromised by MPIO labelling of OECs

OEC viability was compared in MPIO-labelled and unlabelled control cultures by calcein vs ethidium homodimer-1 expression at 24, 48, 72 and 96 h. No adverse effects were observed at any of the above time points, irrespective of MPIO concentration, i.e. OECs retained the MPIO label, migrated normally, retained their spindle morphology and reached confluence (Fig. 4). In the assays in which the PLL surface was mechanically disrupted, MPIO-labelled OEC behaviour was similar to that of unlabelled

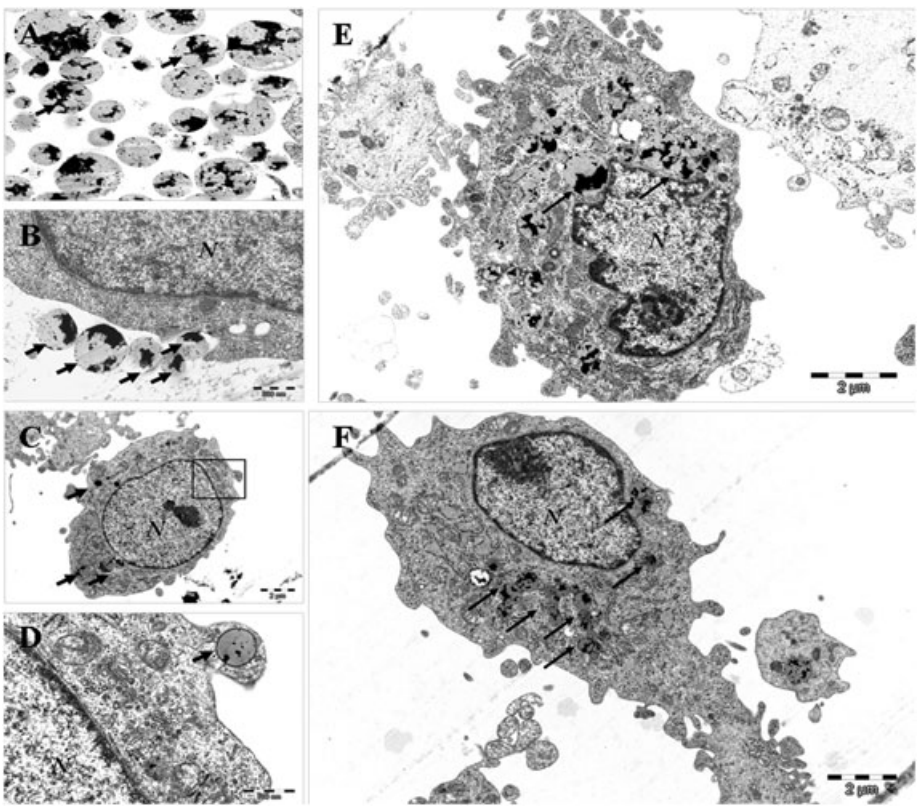

Figure 1. A. TEM of MPIO. Proton-dense regions indicate iron distribution within the particles (arrows). B. MPIO (arrows) in the process of being endocytosed by OEC. C. TEM of OECs with endocytosed MPIO (arrows). D. Higher magnification of region boxed in C, showing recently endocytosed MPIO (arrow). E. TEM of OECs with multiple endocytosed MPIO after 18 h incubation showing perinuclear localisation of MPIO (arrows). F. TEM of OECs with multiple endocytosed MPIO (arrows) after 6 h incubation. N = Nucleus.

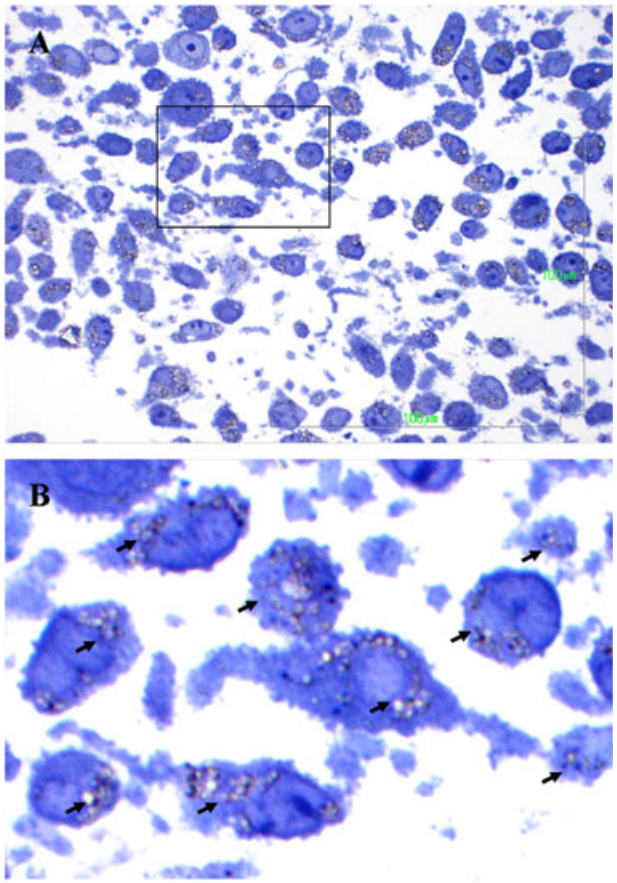

Figure 2. Semi-thin 1 μm-thick section of MPIO-labelled OECS stained with Toluidine Blue showing particles in >90% of the cells. Semi-thin sections enable initial verification of MPIO-labelling before proceeding to further analysis by TEM. B. Higher magnification of region boxed in A showing OECs with mulitple endocytosed MPIO (arrows).

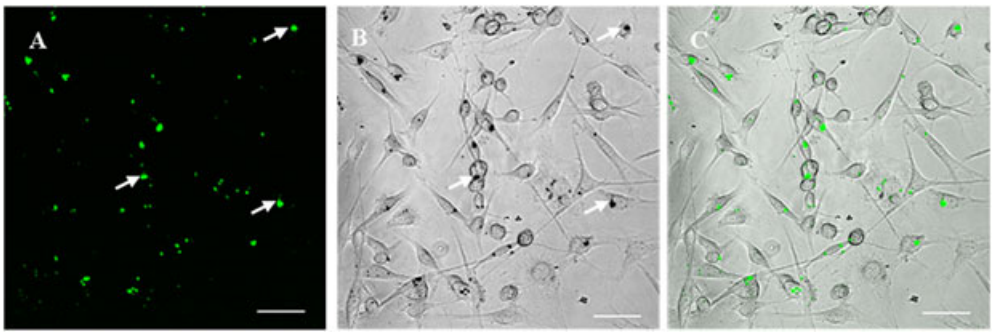

Figure 3. Confocal images of MPIO-labelled OECs after incubation of 12 h. A. Green fluorescence (Dragon Green) derived from endocytosed MPIO (arrows). B. Differential interference contrast (DIC) image of MPIOlabelled OECs, with dense dark regions representing endocytosed MPIO (arrows). C. Merge (A,B).

OECs, i.e. they marginally invaded the artificially created cell-free zone and reached confluence on either side of the zone after 96 h (data not shown).

4.3. MPIO-labelled OECs had normal proliferation rates

Linear regression analysis revealed that the proliferation rates of MPIO-labelled and unlabelled OECs were almost identical (i.e. $R^2 = 0.9857$ and $R^2 = 0.9847$, respectively). Furthermore, passaged MPIO-labelled OECs re-attached to PLL-coated plates and proliferated as normal while proliferation rates were unaffected by the concentration of MPIO used for labelling ($R^2 = \sim 0.98$, irrespective of MPIO label concentration).

4.4. MRI detected multiple and single MPIO-labelled OECs *in vitro* and *in vivo*

MRI of phantoms containing MPIO-labelled cells in different concentrations revealed punctate hypointense regions (Fig. 5). These regions represent susceptibility effects induced by

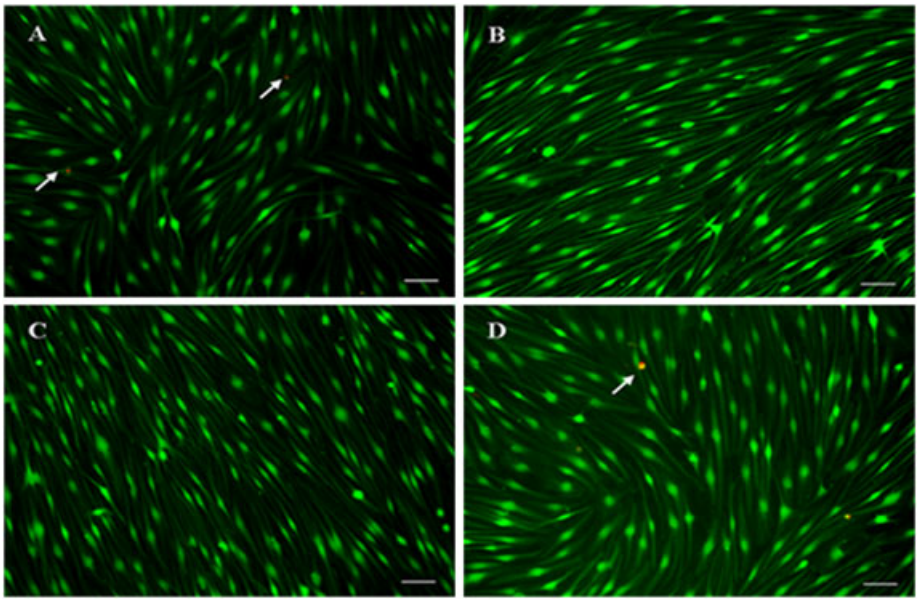

Figure 4. Live/Dead assay 96 h post-MPIO labelling. Live cells express uniform green fluorescence derived from the polyanionic dye calcein. Dead cells and cells with damaged cell membrane express EthD-1 red fluorescence (arrows). MPIO-labelled OECs demonstrate comparable viability profiles to unlabelled controls, while they maintain the same morphological characteristics, migration and proliferation, reaching confluence as normal. A, C. Unlabelled control OECs. B, D. MPIO-labelled OECs at concentrations of 20:1 and 100:1, respectively, 96 h post-labelling, displaying the same characteristics as controls. Scale bars: 10 μm.

endocytosed MPIO. Consistent with expectations, the density of the hypointense regions increased with higher concentrations of both MPIO and MPIO-labelled OECs within the phantom volume (Fig. 5). Given the efficiency of the labelling protocol and the intracellular uptake of MPIO (see above), individual punctate hypointense regions observed are postulated to represent single cells, while variations in hypointensity are attributed to differential uptake of MPIO by individual cells or clustered OECs. No hypointense regions were observed in MR images of phantoms containing unlabelled cells.

In vivo MRI of adult rats detected large intraocular hypointense regions consistent with MPIO-labelled OEC transplants (Fig. 6). No hypointense regions were detected in the contralateral eye of the animals, which received unlabelled OEC grafts. The MPIO-labelled OEC graft was detectable >20 days post-transplantation.

5. DISCUSSION

A pertinent issue in the application of MRI for *in vivo* investigation of transplanted cell behaviour is the development of optimal labelling protocols for specific cell types. Such protocols should enable efficient detection by MRI without compromising viability. Notwithstanding the intense interest in OECs as reparative candidate cells in CNS injury, there are presently only two reported studies in which MRI has been used to detect transplanted OECs (21,22).

In the present study, we have demonstrated that small-diameter MPIO are well suited for efficient labelling of OECs and subsequent detection by MRI without compromising the viability, proliferation and migration of OECs. MPIO of 0.96 μm diameter are endocytosed by OECs, achieving labelling efficiency of >90% after relatively short incubation times of between 6 and 18 h. Individual OECs endocytose multiple MPIO, and individual cells differentially uptake MPIO irrespective of label concentration in all assays.

Previous studies detailing the effects of MPIO on MRI resolution report that the T_2* effects induced by single, 0.76–1.63 μm diameter MPIO are detectable at resolutions of 50 μm and as low as 200 μm (8–10). In our study, differential uptake of 0.96 μm MPIO by individual OECs indicated that the intracellular iron content may vary between cells. However, based on the labelling efficiencies, as well as on detailed microscopic evaluation, we have estimated that, dependent on MPIO:OEC concentration, individual OECs contained a mean of 12–115 MPIO. Thus, particle uptake was great enough for single cell detection by MRI at 7 T at ~100 μm resolution, confirming that the protocol developed in this study is suitable for labelling OECs with MPIO as it can be expected to enable single-cell detection by MRI, even when applying the lowest label concentration (MPIO:OEC = 10:1).

OECs have been labelled in previous studies using MD-100 magnetodendrimers (21) and dextran-coated SPIO particles (22) after 24 and 48 h incubation, respectively. Both studies assessed OEC viability using morphological criteria, trypan blue staining (21), and a propidium iodine exclusion assay (22) carried out immediately after labelling and thus potential longer-term effects of the label on OECs were not addressed. SPIO concentrations of 6 mg ml^{-1} and above were toxic, resulting in the complete loss of the cultured OECs after 48 h incubation (21).

Intracellular labelling with SPIO particles is mediated by either transfection agents or surface modification (5,22) and usually requires long incubation times, typically of 48 h. Thus, a considerable advantage of MPIO over SPIO particles is commercial

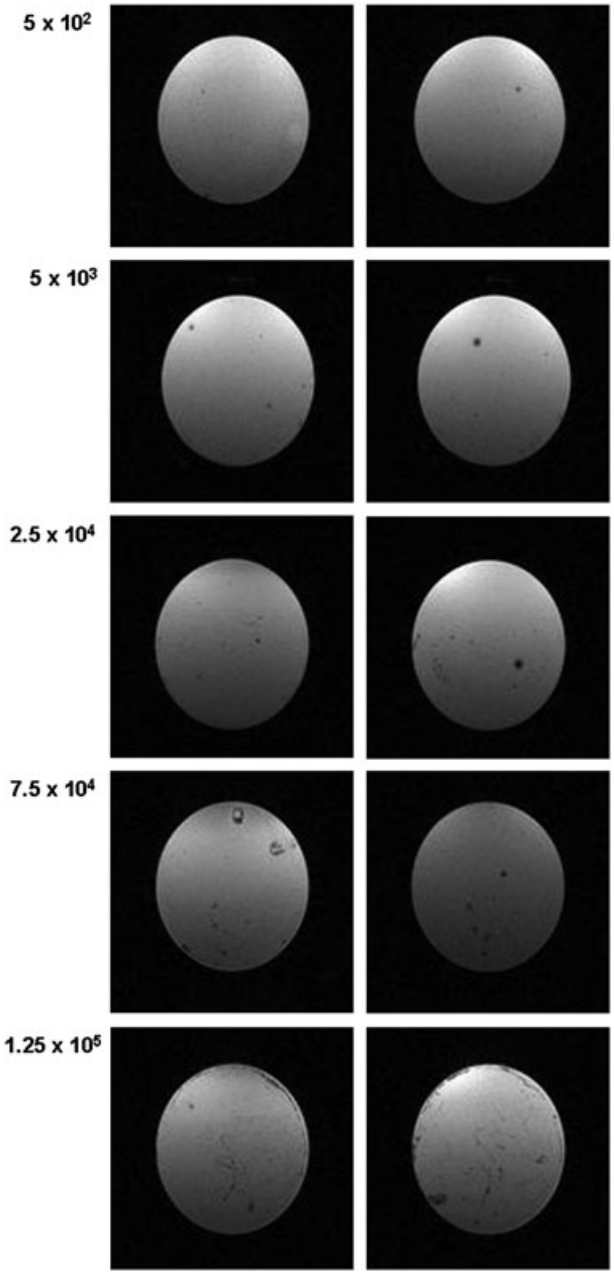

Figure 5. MR images of MPIO-labelled OECs (MPIO:OEC = 10:1) at different concentrations of cells per phantom (indicated in the left column). Punctate hypointense regions are consistent with increasing concentrations of MPIO-labelled cells in the phantoms.

availability and avid endocytosis exhibited by a number of mammalian cells, making the use of transfection agents redundant (7,10,11). Furthermore, cell death induced by high intracellular iron concentrations (21,24–26) constitutes a major concern in the application of iron oxide particles for *in vivo* visualisation by MRI of transplanted cells. In this context, the inert matrix of the MPIO particles may have a protective function compared with biodegradable dextran-coated particles (10). With particular reference to OECs, another consideration is that unlabelled cell survival post-transplantation may on certain occasions be anticipated to be as low as 50% (27). This further emphasizes that *in vitro* labelling of OECs before transplantation should aim at sufficient iron uptake for detection by MRI without adversely affecting cell function. Given that OEC endocytotic uptake cannot be fully controlled under incubation conditions, smaller diameter and lower magnetite content MPIO (i.e. 0.96 μm and 0.125 pg) should be used to reduce the risk of intracellular iron overload.

Endocytosed MPIO are distributed into either endosomes or lysosomes (10,28). To determine the intra-OEC localization of the iron oxide particles, MPIO-labelled OECs were examined by TEM after 6 and 18 h incubation. Heterogeneous uptake of MPIO by individual cells was observed at both time points in all our samples and MPIO were always localized in the cytoplasm. However, an increased peri-nuclear distribution of the particles was observed after prolonged incubation times of $>$18 h.

A series of assays were performed to assess the viability of MPIO-labelled OECs at 24 h intervals after labelling over 4 days. Physical and biochemical properties of MPIO-labelled OECs measured by calcein and resorufin expression, morphological characteristics and motility were the same as those of unlabelled control OECs in identical culture conditions. The specific labelling protocol thus ensures that the viability of MPIO-labelled OECs is the same as that of unlabelled OECs, a property that is particularly important when MPIO-labelled OECs are transplanted *in vivo*. Nevertheless, potential adverse long-term effects of the MPIO label post-transplantation cannot be excluded.

MPIO are fluorescent magnetic polymers used for microscopic verification of intracellular labelling and the tracking of cell movements. Furthermore, the fluorescent label integrated into the iron oxide particles makes histological and immunocytochemical applications possible. However, the presence of fluorescence may confound evaluation of specific assays based on flow cytometry. In the present study, care was taken to apply assay and assessment methods that excluded both spectra interference and data distortions resulting from MPIO fluorescence. Labelling OECs with fluorescent MPIO enables OEC identification in the absence of an unequivocal biomarker (29–31), with the caveat that, in the event of OEC death post-transplantation, the MPIO label may be transferred to *in situ* macrophages and other scavenger cells.

Successful application of MRI in investigations of transplant-mediated CNS repair largely depends on efficiently labelling cells for MRI detection *in vivo*, without compromising their biological properties. MRI of OEC transplants is a powerful tool in experimental and clinical studies of CNS damage and repair for monitoring OEC graft localization and graft/host temporospatial integration. This study presents an assessment of the effects of a widely applied MPIO type specifically on OECs and provides a tested protocol for efficient OEC labelling for tracking their movements with MRI both *in vitro* and after transplantation *in vivo*, without loss of cell viability, proliferation and migration capacity.

Acknowledgements

Special thanks are due to Dr Øystein Riisa for helpful suggestions on phantom design and to Dr Anne Mari Rokstad for expert assistance with confocal microscopy. The work was supported by the Norwegian Research Council, Centre for Research-based Innovation, Medical Imaging Laboratory (grant number 174911/i30).

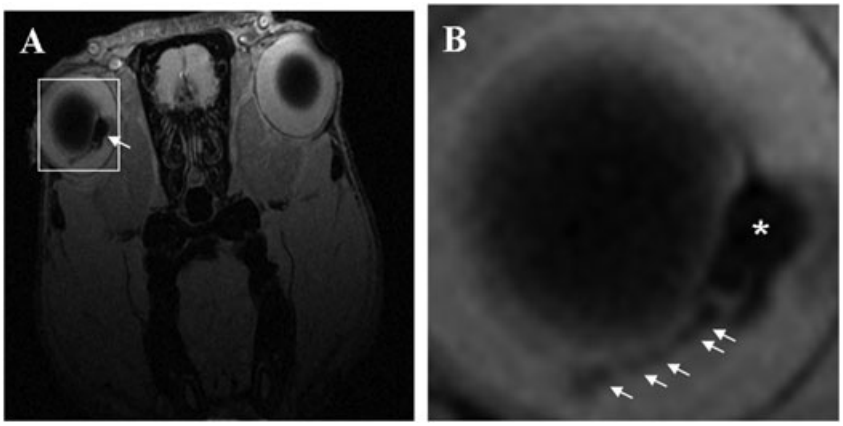

Figure 6. A. *In vivo* MRI of an adult rat showing a dense hypointense region in the vitreous body (arrow) after unilateral intravitreal injection of MPIO-labelled OECs. No hypointense region is observed in the contralateral eye after unlabelled OEC injection. B. Higher magnification of area boxed in A showing intravitreal cell graft (asterisk) and trail of small clusters/single MPIO-labelled OECs (arrows) consistent with site of intravitreal injection.

REFERENCES

1. Slotkin JR, Cahill KS, Tharin SA, Shapiro EM. Cellular magnetic resonance imaging: nanometer and micrometer size particles for non-invasive cell localisation. Neurotherapeutics 2007; 4: 428–433; doi:10.1016/j.nurt.2007.05.010
2. Ye Q, Yang DW, Williams M, Williams DS, Pluempitiwiriyawej C, Moura JM, Ho C. In vivo detection of acute rat renal allograft rejection by MRIO using USPIOs. Kidney Int 2002; 61: 1124–1135; doi:10.1046/j.1523-1755.2002.00195.x
3. Beckman N, Cannet C, Fringeli-Tanner M, Baurmann D, Pally C, Bruns C, Zerwes HG, Andriambeloson E, Bigaud M. Macrophage labelling by SPIO as an early marker of allograft chronic rejection a rat model of kidney transplantation. Magn Reson Med 2003; 49: 459–467; doi:10.1002/mrm.10387
4. Rausch M, Sauter A, Fröhlich J, Neubacher, et al. Dynamic patterns of USPIO enhancement can be observed in macrophages after ischemic brain damage. Magn Reson Med 2001; 46: 1018–1022; doi:10.1002/mrm.1290
5. Frank JA, Miller BR, Arbab AS, Zywicke HA, Jordan EK, Lewis BK, Bryant LH Jr, Bulte JW. Clinically applicable labelling of mammalian and stem cells by combining superparamagnetic iron oxides and transfection agents. Radiology 2003; 228: 480–487; doi:10.1148/radiol.2281020638
6. Yeh TC, Zhang W, Ilstad ST, Ho C. In vivo dynamic MRI tracking of rat T-cells labelled with superparamagnetic iron oxide particles. Magn Reson Med 1995; 33: 200–208.
7. Hinds KA, Hill JM, Shapiro EM, Laukkanen MO, Silva AC, Combs CA, Varney TR, Balaban RS, Koretsky AP, Dunbar CE. Highly efficient endosomal labelling of progenitor and stem cells with large magnetic particles allows magnetic resonance imaging of single cells. Blood 2003; 102: 867–872; doi:10.1182/blood-2002-12-3669
8. Shapiro EM, Skrtic S, Sharer K, Hill JM, Dunbar CE, Koretsky AP. MRI detection of single particles for cellular imaging. Proc Natl Acad Sci USA 2004; 101: 10901–10906; doi:10.1073/pnas.0403918101
9. Shapiro EM, Skrtic S, Koretsky AP. Sizing it up: cellular MRI using micron sized iron oxide particles. Magn Reson Med 2005; 53: 329–338; doi:10.1002/mrm.20342
10. Shapiro EM, Sharer K, Skrtic S, Koretsky A. In vivo detection of single cells by MRI. Magn Reson Med 2006; 55: 242–249; doi:10.1002/mrm.20718
11. Williams JB, Ye Q, Hitchens K, Kaufman C, Ho C. MRI detection of macrophages labelled using micrometer-sized iron oxide particles. J Magn Reson Imag 2007; 25: 1210–1218; doi:10.1002/jmri.20930
12. Doucette R. PNS-CNS transitional zone of the first cranial nerve. J Comp Neurol 1991; 312: 451–466.
13. Barnett SC, Riddell JS. Olfactory ensheathing cells (OECs) and the treatment of CNS injury: advantages and possible caveats. J Anat 2004; 204: 57–67; doi:10.1111/j.1469-7580.2004.00257.x
14. Moreno-Flores MT, Díaz-Nido J, Wandosell F, Avilla J. Olfactory ensheathing glia: drivers of axonal regeneration in the central nervous system? J Biomed 2002; 2: 37–43; doi:10.1155/S1110724302000372
15. Franklin RJM. Remyelination by transplanted olfactory ensheathing cells. Anat Rec 2003; 271B: 71–76; doi:10.1002/ar.b.10013
16. Ramon-Cueto A, Cordero MI, Santos-Benito F, Avila J. Functional recovery of paraplegic rats and motor axon regeneration in their spinal cords by olfactory ensheathing cells. Neuron 2000; 25: 425–435; doi:10.1016/S0896-6273(00)80905-8
17. Raisman G. Repair of spinal cord injury by transplantation of olfactory ensheathing cells. C R Biol 2007; 330: 557–560; doi:10.1016/j.crvi.2007.03.010
18. Sandvig A, Sandvig I, Berry M, Olsen Ø, Pedersen TB, Brekken C, Thuen M. Axonal tracing of the normal and regenerating visual pathway of mouse, rat, frog, and fish using manganese-enhanced MRI (MEMRI). J Magn Reson Imag 2011; doi:10.1002/jmri.22631
19. Thuen M, Berry M, Pedersen TB, Goa PE, Summerfield M, Haraldseth O, Sandvig A, Brekken C. Manganese-enhanced MRI of the rat visual pathway: acute neural toxicity, contrast enhancement, axon resolutionm axonal transport, and clearance of Mn2+. J Magn Reson Imag 2008; 4: 855–865; doi:10.1002/jmri.21504
20. Berry M, Carlile A, Hunter A, Tsang W-L, Rosustrel P, Sievers J. Optic nerve regeneration after intravitreal peripheral nerve implants: trajectories of axons regrowing through the optic chiasm into the optic tracts. J Neurocytol 1999; 28: 721–741.
21. Lee I-H, Bulte JWM, Schweinhardt P, Douglas T, Trifunovski A, Hofstedder C, Olson L, Spenger C. In vivo magnetic resonance imaging of olfactory ensheathing glia grafted into the rat spinal cord. Exp Neurol 2004; 187: 509–516; doi:10.1016/j.expneurol.2004.02.007
22. Dunning MD, Lakatos A, Loizou L, Kettunen M, Ffrench-Constant C, Brindle KM, Franklin RJ. Superparamagnetic iron oxide labelled Schwann cells and olfactory ensheathing cells can be traced in vivo by magnetic resonance imaging and retain functional properties after transplantation into the CNS. J Neurosci 2004; 24: 9799–9810; doi:10.1523/JNEUROSCI.3126-04.2004
23. Barnett SC, Roskams AJ. Olfactory ensheathing cells: isolation and culture from the neonatal olfactory bulb. Meth Mol Biol 2008; 438: 85–94.
24. Zhao M, Kircher MF, Josephson L, Weissleder R. Differential conjugation of tat peptide to superparamagnetic nanoparticles and its effect on cellular uptake. Bioconjug Chem 2002; 228: 840–844; doi:10.1021/bc0255236
25. Riley MR, Boesewetter DE, Kim AM, Sirvent FP. Effects of metal Cu, Fe, Ni, V, and Zn on rat lung epithelial cells. Toxicology 2003; 190: 171–184.
26. Bishop GM, Robinson SR. Quantitative analysis of cell death and ferritin expression in response to cortical iron: implications for hypoxia–ischemia and stroke. Brain Res 2001; 907: 175–187; doi:10.1016/S0006-8993(01)02303-4
27. Barnett SC, Riddell JS. Olfactory ensheathing cell transplantation as a strategy for spinal cord repair – what can it achieve? Nat Clin Pract Neurol 2007; 3: 152–161.
28. Shapiro EM, Medford-Davis LN, Fahmy TM, Dunbar CE, Koretsky AP. Antibody-mediated cell labelling of peripheral T cells with

micron-sized iron oxide particles (MPIOs) allows single cell detection by MRI. Contrast Media Mol. Imag 2007; 2: 145–153; doi:10.1002/cmmi.134
29. Tomé M, Siladžic E, Santos-Silva A, Barnett SC. Calponin is expressed by subpopulations of connective tissue cells but not olfactory ensheathing cells in the neonatal olfactory mucosa. BMC Neurosci 2007; 8: 74; doi:10.1186/1471-2202/8/74
30. Ibanez C, Ito D, Zawadzka M, Jeffery ND, Franklin RJM. Calponin is expressed by fibroblasts and meningeal cells but not olfactory ensheathing cells in the adult peripheral olfactory system. Glia 2007; 55: 144–151; doi:10.1002/glia.20443
31. Smithson LJ, Kawaja MD. A comparative examination of biomarkers for olfactory ensheathing cells in cats and guinea pigs. Brain Res 2009; 1284: 41–53; doi:10.1016/j.brainres.2009.06.011